Eco-Environment & Health 4 (2025) 100122

Contents lists available at ScienceDirect

Eco-Environment & Health

journal homepage: www.journals.elsevier.com/eco-environment-and-health

Original Research Article

Molecular modeling to elucidate the dynamic interaction process and aggregation mechanism between natural organic matters and nanoplastics

Chi Zhang [a,b,1], Zhiyu Zhou [a,1], Mengning Xi [a], Haozhe Ma [a], Junhao Qin [c,*], Hanzhong Jia [a,b,*]

[a] College of Natural Resources and Environment, Northwest A & F University, Xianyang 712100, China
[b] Key Laboratory of Low-Carbon Green Agriculture in Northwestern China, Ministry of Agriculture and Rural Affairs, Xianyang 712100, China
[c] Guangdong Laboratory for Lingnan Modern Agriculture, Guangdong Provincial Key Laboratory of Agricultural & Rural Pollution Abatement and Environmental Safety, College of Natural Resources and Environment, South China Agricultural University, Guangzhou 510642, China

ARTICLE INFO

Keywords:
Natural organic matters
Aged nanoplastics
Interaction processes
Aggregation mechanism
Molecular modeling

ABSTRACT

The interactions of nanoplastics (NPs) with natural organic matters (NOMs) dominate the environmental fate of both substances and the organic carbon cycle. Their binding and aggregation mechanisms at the molecular level remain elusive due to the high structural complexity of NOMs and aged NPs. Molecular modeling was used to understand the detailed dynamic interaction mechanism between NOMs and NPs. Advanced humic acid models were used, and three types of NPs, i.e., polyethylene (PE), polyvinyl chloride (PVC), and polystyrene (PS), were investigated. Molecular dynamics (MD) simulations revealed the geometrical change of the spontaneous formation of NOMs-NPs supramolecular assemblies. The results showed that pristine NPs initially tend to aggregate homogeneously due to their hydrophobic nature, and then NOM fragments are bound to the formed NP aggregates mainly by vdW interaction. Homo- and hetero-aggregation between NOMs and aged NPs occur simultaneously through various mechanisms, including intermolecular forces and Ca^{2+} bridging effect, eventually resulting in a mixture of supramolecular structures. Density functional theory calculations were employed to characterize the surface properties and reactivity of the NP monomers. The molecular polarity indices for unaged PE, PS, and PVC were 3.1, 8.5, and 22.2 kcal/mol, respectively, which increased to 43.2, 51.6, and 42.2 kcal/mol for aged NPs, respectively, indicating the increase in polarity after aging. The vdW and electrostatic potentials of NP monomers were visualized. These results clarified the fundamental aggregation processes, and mechanisms between NPs and NOMs, providing a complete molecular picture of the interactions of nanoparticles in the natural aquatic environment.

1. Introduction

Natural organic matters (NOMs) play a critical role in a variety of (bio)geochemical processes in natural water environments by directly affecting microbial activity, co-aggregation, contaminant retention, water quality, and element cycling. The environmental behaviors of NOMs are also closely related to the global carbon cycle and climate change by preserving and converting organic carbon [1,2]. Despite their importance, a thorough and precise understanding of NOMs' composition and structure is still lacking. Structurally, NOM is extremely complex and heterogeneous as a supramolecular mixture of chemically distinct organic compounds that are abundant in chemically diverse functional groups and active sites. The major functional groups in NOM have long been clearly identified, such as carboxylic, phenolic, alcoholic, carbonyl, amino, etc. The compositional complexity and structural diversity of NOMs present a severe challenge to experimental characterization and building of realistic models, but nowadays computational chemistry methods have made this problem tractable [3–5].

In nature, NOMs interact closely with organic pollutants through mechanisms such as adsorption, co-precipitation, and homogeneous/heterogeneous aggregation through different mechanisms such as π–π interaction, hydrophobic interaction, H–bonding, electrostatic attraction, steric hindrance effect, and so forth [6], thus governing the environmental fate of pollutants and profoundly impacting the distribution and preservation of organic carbon. Nanoplastics (NPs), as a class of emerging contaminants, have a particle size between 1 nm and 100 nm

* Corresponding authors.
E-mail addresses: J_Qin@scau.edu.cn (J. Qin), jiahz@nwafu.edu.cn (H. Jia).
[1] Contributed equally to this work.

https://doi.org/10.1016/j.eehl.2024.08.004
Received 24 May 2024; Received in revised form 25 August 2024; Accepted 30 August 2024
Available online 11 September 2024

[7] and are generated from plastic production by natural or anthropogenic factors, such as photooxidation and microbial degradation [8,9]. Due to their chemical stability, persistence, and bioaccumulation, the environmental behaviors of NPs, in particular their interactions with different environmental pollutants during their transport through the marine or sedimentary environment into ecosystems, have received considerable research attention in recent years [10–13]. Compared to microplastics (MPs, <5 mm), the molecular-level properties and environmental implications of NPs in natural systems have been relatively less studied because of methodological challenges. For instance, it is still technically challenging to extract NPs from natural environments, and their surface properties are not clearly identified [14–17]. There is also research suggesting that NPs are more abundant and hazardous in the environment than MPs [18]. The transport and fate of NPs are greatly determined by interactions with environmental media, such as aggregation with NOMs and deposition onto minerals' surfaces [19–22]. Therefore, it is imperative to understand the environmental processes and behaviors of NPs with environmental media, thus providing significant implications for their ecological risk assessment.

The interactions between NOMs and NPs are of fundamental importance and largely control the environmental fate of both materials, as well as the stabilization and cycling of organic carbon in nature [23]. NOMs can have an impact on the transport and distribution of NPs in the aquatic environment, because the presence of NOMs can alter the surface properties of NPs, affecting their aggregation and mobility [24]. NOM can also be adsorbed onto the surface of NPs, changing their chemical reactivity and affecting the adsorption of other contaminants, such as metals and organic pollutants, onto the NP surface [25]. Furthermore, the evaluation of the effect of NOMs on the behaviors of NPs was the first critical step in assessing the potential environmental hazards of NPs in ecosystems. However, a detailed molecular-level picture of the dynamic interaction processes and the underlying mechanism between NOMs and NPs is still elusive. It is difficult to directly observe and decipher the complicated NOM–NP aggregating behaviors only relying on traditional experimental techniques. There is an urgent need for a better understanding of such processes that can provide more quantitative information, such as the determination of fundamental mechanisms (homo–aggregation or hetero–aggregation), identification of active sites, observation of dynamic aggregation processes, and characterization of binding and aggregating structures.

With the rapid development of theoretical and computational chemistry and computer hardware, computational simulations have been proven an essential and powerful approach in quantitatively revealing aqueous environmental processes and reactions at the molecular scale beyond the conventional resolution of analytical methods, based on the identification and analysis of a range of physicochemical properties, such as geometrical characteristics, thermodynamics, electronic structures, and dynamics of substances [5,26–33]. For example, Xue et al. [34] reviewed the application of computational modeling methods at various scales in understanding the interface behavior of pollutants, especially in aquatic environments. Li et al. [31] reviewed recent progress in using environmental theoretical calculations to elucidate the transformation mechanisms of contaminants. In addition, this group has extensively revisited the application of density functional theory (DFT) calculations to the prediction of active sites and reaction selectivity, as well as oxidant activation mechanisms in the field of advanced oxidation processes (AOPs) [30]. However, research providing deep insights into the interactions between NOMs and NPs has rarely been conducted using theoretical calculation methods. In a recent study, the dynamic properties and microscopic aggregation structures related to the NPs-NOMs assemblage were studied by molecular dynamics (MD) simulations, which acquired deep insights into the interparticle interactions between both substances [35]. However, this study only incorporated virgin plastics, and the aged forms of NPs were not considered. According to previous research [23,36–38], oxygen-containing functional groups, including carboxyl, phenolic, and carbonyl groups, are generated after aging, which leads to the modification of the surface morphology of MPs, such as specific surface area and roughness. Therefore, it can be expected that different surface properties of aged NPs would lead to more significant and interesting phenomena and aggregation mechanisms with NOMs in comparison to pristine NPs, given that NOMs have a high degree of structural complexity and heterogeneity, the chemical composition of which is very diverse, and aged NPs also have a wide variety of O–containing functional groups.

In the present study, by performing MD simulations and DFT calculations, we explored the dynamic interactions and elucidated the detailed molecular-level mechanism between NOMs and three types of NPs, polyethylene (PE), polyvinyl chloride (PVC), and polystyrene (PS) in both pristine and aged form. The dynamic binding and aggregation processes between two substances are qualitatively revealed by the movement trajectories and statistical data. Analysis of the interaction energies between NOM and NP fragments and characterization of the direct intermolecular binding and local coordination geometries of Ca^{2+} bridging provides a profound insight into the aggregation mechanism. DFT calculations allow a quantitative analysis of the reactivity and active sites of NPs, and weak interactions between NOM and PS fragments are presented visually. These results establish a fundamental basis for the understanding of the fate of NPs in the aquatic environment and the stabilization of organic C.

2. Methodology

2.1. Computational models

2.1.1. Leonardite humic acid

Vienna Soil Organic Matters Modeler 2 (VSOMM2) is an online tool to generate theoretical models of humic substances [39,40] based on the data derived from standardized samples of the International Humic Substances Society (IHSS). The NOMs condensed phase models constructed by VSOMM2 fundamentally rely on the concept of building blocks (BBs), which represent the simple units in organic components, and the implementation of a genetic algorithm randomly results in the chemical and structural diversity of the final models. On this website, the primary elemental composition and organic carbon fractions are required as input, and the modeler calculates and generates a diverse combination of heterogeneously distributed NOM fragments automatically that match the input.

In this study, VSOMM2 was used to build theoretical models of the supramolecular structure of Leonardite humic acid (LHA) according to the elemental and organic composition of the IHSS. LHA has been extensively used in the molecular modeling of NOMs in previous studies [5,27]. The created LHA model was composed of 100 building blocks with 10 building blocks per molecule. The detailed element and organic composition of the generated LHA are listed in Table S1. The molecular geometries of the 10 deprotonated NOM fragments are illustrated in Fig. S1. These molecules collectively constitute the NOMs' supramolecular association.

2.1.2. Nanoplastics

Both pristine and aged NPs (Fig. S2) were investigated in our simulations with the purpose of clarifying the effect of oxygen-containing functional groups on aggregation behaviors. Each monomer of the PE and PVC chain had a degree of polymerization of 10, and each PS monomeric chain contained 5 polymerized units. There were 16 such NP monomers in each simulation system. For pristine NPs, the models we used were similar to those in previous studies. For aged NPs, due to their structural complexity, the models have not yet been developed, so we had to use the simplified models. Simplified models of aged NPs were constructed by incorporating O-containing functional groups according to previous studies [35,41]. In brief, each monomer contained four carbonyls, two hydroxyls, and one carboxyl. The carboxylic groups of NOM and NP fragments were deprotonated (in a circumneutral environment) due to the relatively low pK_a of these groups. Each monomeric chain of

aged NPs possessed a net charge of −1, and the 10 NOM fragments had different negative charges depending on the number of carboxylate groups.

2.1.3. Simulation systems

NOMs–NPs coexisting binary systems (Fig. 1) were constructed. NOMs and NPs molecules were initially placed at random positions within the simulation cell. This setup was designed to enable the direct observation of the spontaneous aggregation processes of both materials. Alternatively, one can first build a homo-aggregate of NP nanoparticles, then possibly age its surface, and then insert these NOM molecules into the solution. This setup should be more reasonable but also more complicated and therefore not adopted in this work. Moreover, to clearly reveal the effect of their interactions on the behaviors of both NOMs and NPs, unary systems that contained only NOMs or NPs were also simulated. There were 13 individual simulation systems in all: 6 binary systems and 7 unitary systems. For each system, NOM/NP fragments were first randomly distributed in the simulation box (approximately 76.5 Å × 76.5 Å × 76.5 Å), and then salt ions and solvent water molecules were randomly placed in the region to simulate the solution environment. It is well known that Ca^{2+} and Na^{+} are the most common salt ions. Therefore, Ca^{2+} ions were added to counterbalance the net negative charges from NOMs and aged NPs, and additionally ~0.1 mol/L NaCl was added in each system. The detailed compositions of all the systems are summarized in Table S2. All of the simulation cells were periodically repeated.

2.2. MD setup

All MD simulations were carried out by GROMACS 2018.4 [42]. Amber 03 force field [43] was used to describe interatomic interactions. A cutoff value of 12 Å was used for short-range electrostatic and van der Waals (vdW) interactions. The particle mesh Ewald (PME) summation method [44] was employed for the summation of long-range electrostatic interactions. The SPC/E water model was used [45]. The rigidity of water was constrained by the LINCS algorithm [46]. The atomic charges were derived by DFT calculations (see the details in *Section 2.3*).

The propagation of Newtonian equations of motion was realized via the leap-frog algorithm. Berendsen barostat [47] and velocity-rescale thermostat [48] were employed to maintain the pressure and temperature, respectively. For each simulation, we first performed a pre-equilibration for 0.5 ns in the NVT ensemble at 298 K and then 1–2 ns equilibration in the NPT ensemble at 1 atm and 298 K. Subsequently, a production run for 100 ns with a timestep of 2 fs in NVT ensemble was carried out. Data of the last 20 ns were used for statistics.

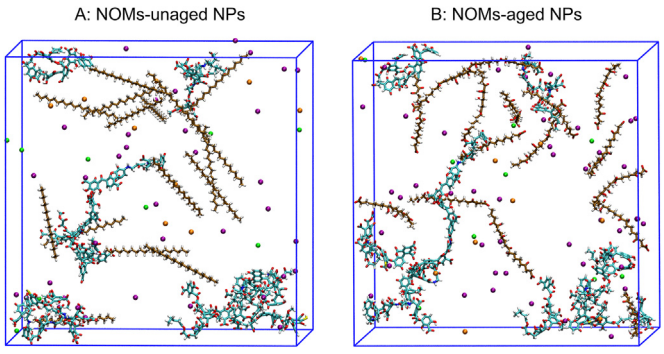

Fig. 1. Computational models of original systems used for MD simulations. NOMs and NPs fragments are shown as sticks; salt ions are represented by balls. Color code: N = blue; H = white; O = red; S = yellow; Na = green; Ca = purple; Cl = orange. The C in NOMs and NPs are colored by cyan and brown, respectively. The water molecules are not shown for clarity. MD, molecular dynamics; NOMs, natural organic matters; NPs, nanoplastics.

2.3. DFT calculations for surface reactivity

DFT calculations were used to give a more comprehensive understanding of the interaction mechanism at atomic and electronic scales. All of the quantum chemistry calculations were conducted by the Gaussian 16 program. The geometry optimizations of the 6 monomeric chains of NPs (i.e., pristine and aged PE, PVC, and PS) and 10 individual NOM fragments were performed at the quantum chemistry level of def2-TZVP basis set [49] and B3LYP functional [50,51], complemented by DFT–D3 dispersion correction [52]. The partial atomic charges of all the NOMs and NP monomers were derived by the Multifwn 3.8 program [53]. The acquired RESP2 (0.5) atomic charges [54] were used in MD simulations.

Several key descriptors were analyzed on the basis of the structures and wavefunctions by Multifwn 3.8 [53], including electrostatic potential (ESP), vdW potential, and molecular polarity index (MPI) of NP monomers. ESP is quite common and useful for intuitively disclosing possible electrostatic interaction of the investigated chemical entity with the external environment, and ESP is usually mapped on an electron density isosurface of 0.001 a.u. [55]. Due to the low polarity of pristine NPs, their vdW interaction deserves more attention than electrostatic interactions. As a new real space function that is similar to ESP, vdW potential can visually reflect the vdW interaction between a chemical system and the external environment [56]. The advantage of MPI is that it quantifies local polarity induced by the non-uniform distribution of ESP, which is a better descriptor compared to dipole moment that only depicts overall polarity.

2.4. Weak interaction analysis and visualization

An independent gradient model based on the Hirshfeld partition (IGMH) of the molecular density method [57] can help to graphically display the weak interactions between two fragments in a complexing system. In order to analyze the nature and region of interaction between NOM and NP fragment, a configuration of a typical NOM–NP dimer was optimized by DFT static calculations in a non-periodic system, and IGMH analysis was performed subsequently by Multifwn 3.8 [53]. All of the isosurface maps were shown and rendered by VMD software [58].

The geometry optimization of the dimer was conducted with the CP2K/QUICKSTEP package [59], which was based on a mixed Gaussian and plane waves (GPW) approach [60]. PBE exchange–correlation functional [61], DZVP basis sets [62], and GTH pseudopotentials [63] were applied. The electronic density cutoff was 500 Ry. L–BFGS optimizer [64] was adopted, and convergence criteria for maximum force and displacement were set to be 0.0001 and 0.001 a.u., respectively. Self-consistent continuum solvation (SCCS) implicit solvent model [65] and Grimme's DFT–D3 dispersion correction [52] were employed.

3. Results and discussion

3.1. Dynamic aggregation processes and structures

3.1.1. Unitary systems

For unitary systems, the solvent-accessible surface areas (SASAs) as a function of the simulation time of individual NOMs and NPs fragments are shown in Fig. S3. One can observe an overall tendency that all the SASAs are decreasing with simulation time, which indicates the dynamic homo–aggregation processes with the formation of large supramolecular structure (Fig. S4). Notably, the hydrophobic areas of the unaged NPs decreased markedly and remained stable in later simulations, indicating the importance of hydrophobic forces in the self-assembly of the NPs. As NPs molecules come into contact, the water molecules between them are expelled into the bulk due to the weaker interactions between water and hydrophobic surfaces, compared to interactions with other solvents, which is considered an entropy-driven process [66]. Simulation trajectories clearly show that separate NP monomers move toward each other spontaneously and ultimately form a compact cluster. For pristine NPs, it

is evident that hydrophobic regions make a dominant contribution to the total SASA, while hydrophilic areas make up only a very small proportion (Fig. S3A, C, E), due to the hydrophobic nature of unaged NPs surfaces. Pristine PE homo–aggregate, the least hydrophilic area, is nearly zero (Fig. S3A). In contrast, PVC polymer shows the largest hydrophilic areas, possibly due to the slight polar property induced by Cl atoms in alkyl chains (Fig. S3C), which is consistent with a previous study [44]. In contrast, the hydrophilic areas of aged NPs homogeneous agglomerates (Fig. S3B, D, F) are significantly larger than those of unaged NPs. This phenomenon provides evidence that the oxygen-containing functional groups endow hydrocarbon molecules with partial hydrophilic characteristics. All three types of pristine NPs formed stable aggregate structure of a large aggregate (Fig. S4A, C, E) driven mainly by hydrophobic interaction.

Similar to pristine NPs, the supramolecular aggregate of aged NPs homo–aggregate is gradually formed with the movement of the whole system. Aged PE ultimately evolved into several small clusters (Fig. S4B) that are less compact compared to the large supramolecular architecture formed by PVC and PS (Fig. S4D and F). Furthermore, the homo–aggregation of aged NPs proceeds through more complicated mechanisms than unaged NPs: hydrophilic (e.g., H–bonding), hydrophobic, and cation bridging (via Ca^{2+}) collectively contribute to the homo–aggregation of aged NPs in a water environment. In the unitary system of NOMs, the aggregation of LHA molecules occurs gradually, first by forming close contacts and then by the chelation of functional groups to form a co-aggregate (Fig. S4G), and its aggregation mechanism has been discussed at great length in previous MD studies [3,67–69].

3.1.2. *Binary systems*

The root-mean-square deviation (RMSD) curves of NOMs-NPs associations as a function of simulation time are presented in Fig. S5. The curves show that the RMSD values stabilize at approximately 4.5 nm after 40 ns, indicating that the sampling is sufficient. The variations of SASAs of NOMs–NPs associations over simulation time in binary systems are shown in Fig. 2, which manifest the gradual aggregation processes of NOMs and NPs mixtures for all systems. In the initial configurations, the fragments of NOMs and NPs are arranged in a random manner, and no significant interactions are observed between these fragments. As the system moves, the distances between the NOMs and NPs decrease, driven by the gradual increase in intermolecular forces and H-bonding interactions, eventually leading to aggregation. Fig. 3 illustrates the microscopic geometric configurations of the formed NOMs–NPs aggregates. For the NOMs-pristine PE system, all of the PE monomers aggregate to form a small particle with a pillar-like geometry. In this structure, the alkane chains are bundled together and aligned parallel to each other through hydrophobic interactions. Subsequently, NOM fragments or small clusters are adsorbed onto the external surface of the PE polymer through their hydrophobic groups. Such a heterogeneous aggregation mechanism, triggered by the simultaneous adsorption of NOMs and homogeneous aggregation of NPs, results in the formation of a pristine NOMs-NPs PE aggregate (Fig. 3A). In this structure, the outer NOMs expose their hydrophilic functional groups to the external aqueous environment, exhibiting a high binding affinity to metal cations and polar organic substances. In comparison, substantial heterogenous aggregation occurs between NOMs and aged PE fragments due to the increased hydrophilicity of PE. As a result, aged PE and NOMs directly form hetero–aggregating structures through intermolecular interactions and cation bridging (Fig. 3B). For NOMs–pristine PVC binary system, both substances polymerize individually to form separate clusters, and then the two homo–aggregates are bound together primarily through non-polar moieties (Fig. 3C). As shown in Fig. 3D, the case for aged PVC is slightly different: the large cluster of aged PVC and supramolecular aggregate of NOMs have less significant interaction in which a small portion of the deprotonated carboxyl groups of aged PVC and NOMs are bridged by Ca^{2+}. For NOMs, which are pristine PS binary systems, the formed agglomerate is structurally similar to that of NOMs–pristine PE assemble. That is, PS monomers aggregate by hydrophobic force and intense π–π stacking, and then separate NOM clusters with different geometries bind to their outer surface by intermolecular interactions (Fig. 3E). NOMs and aged PS directly form a large heterogeneous

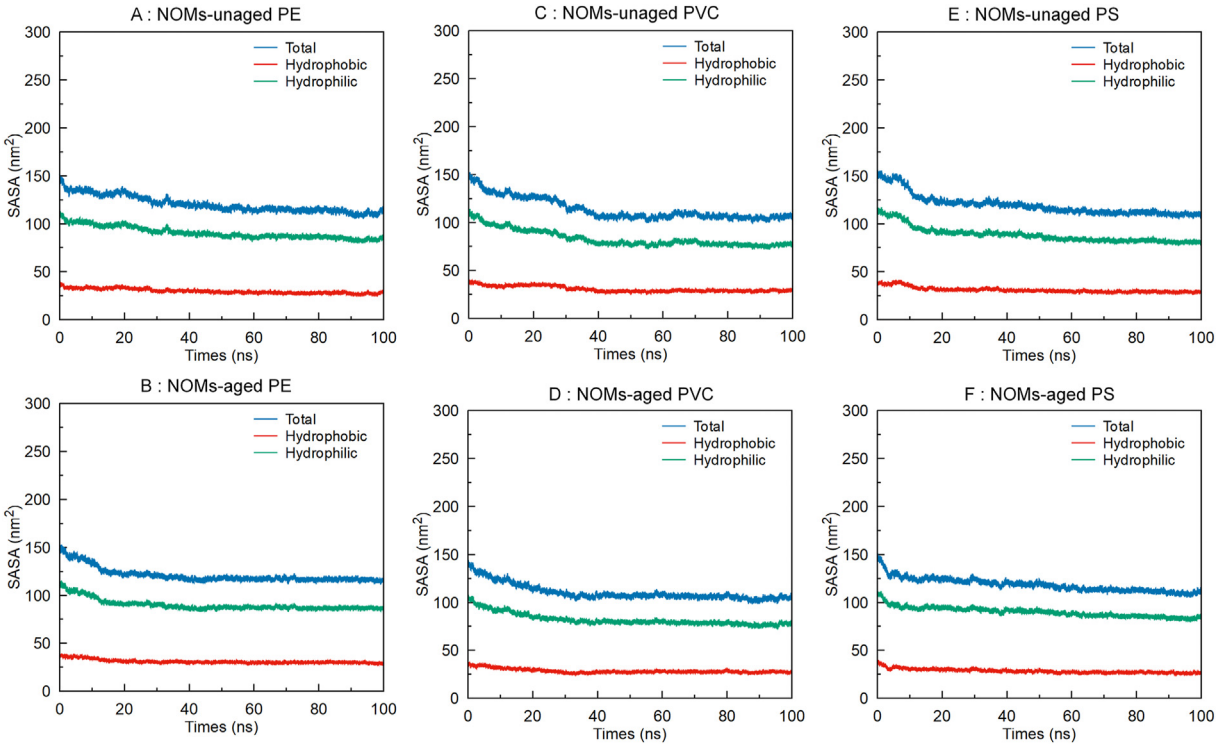

Fig. 2. Time evolution of solvent accessible surface areas (SASAs) of NOMs–NPs associations in binary systems. PE, polyethylene; PVC, polyvinyl chloride; PS, polystyrene.

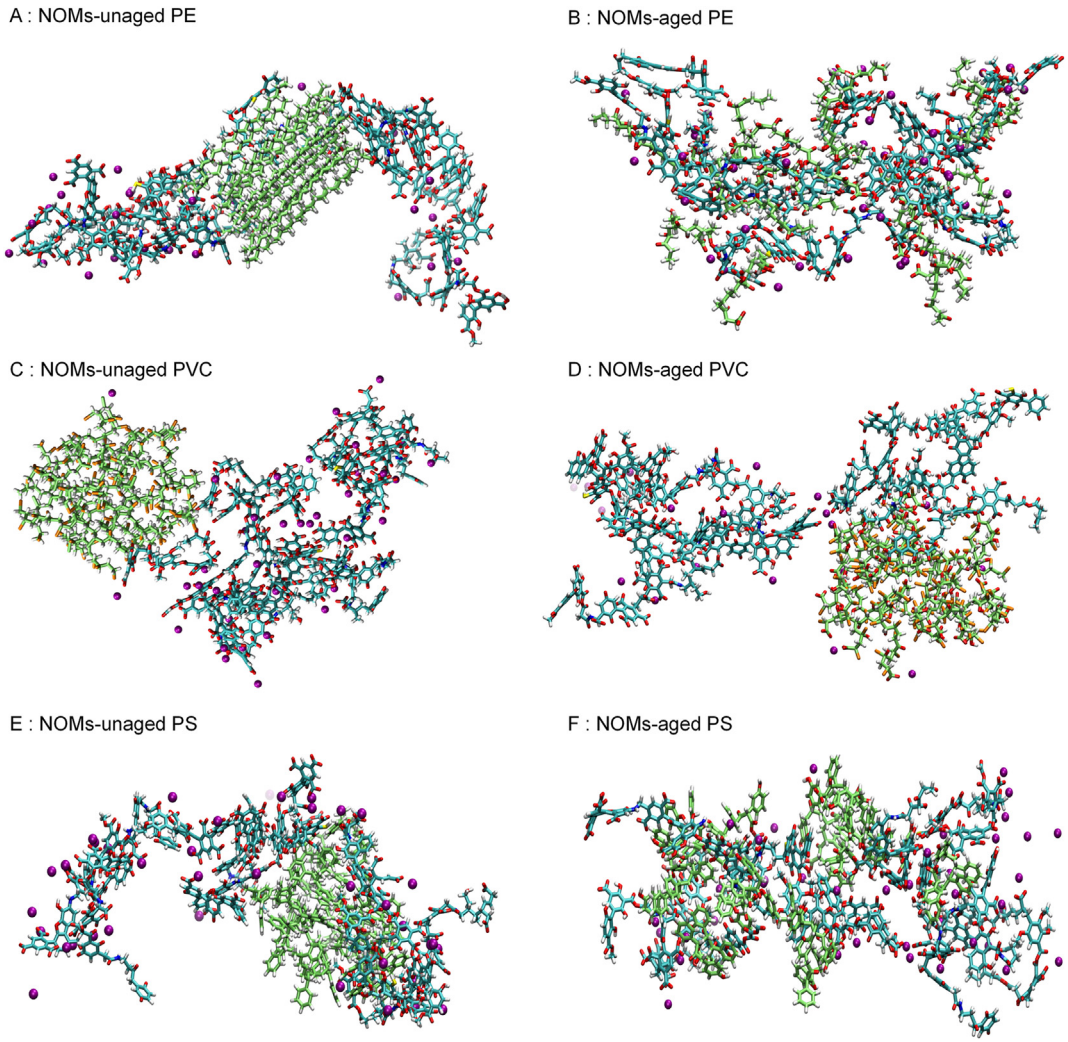

Fig. 3. Snapshots of NOMs–NPs heterogeneous aggregating clusters in binary systems. Coloring code: N = blue; H = white; O = red; S = yellow; Ca = purple; Cl = orange. Carbon atoms in NOMs and NPs are depicted in cyan and green, respectively.

aggregate in which fragments of both materials are joined mainly by cation bridging (Fig. 3F), similar to the case for NOMs-aged PE aggregate described above. A recent study has demonstrated that as the adsorption time increases, the FTIR peak intensities of PS and PE exhibit an upward trend, while those of PVC show no obvious change, indicating that the binding interaction between PVC and NOMs is different from others [70]. This finding is consistent with the obtained microscopic architectures of NPs–NOMs aggregates. In addition, it has been deduced that if the surface sites of MPs are not rich enough, NOM molecules will first occupy the adsorption sites on the surface of pristine MPs and then bind to NOMs already retained on the MP, i.e., the multilayer adsorption mode, but if there are sufficient binding sites on the surface of MPs, HA will tend to be bound as a single layer [71]. In our simulations, the binding of NOMs to NPs shows a structure more resembling multilayer adsorption, possibly due to the similar size of both substances.

To better visualize the microscopic aggregation structures, the solvent water molecules are not shown in the snapshots. In fact, these water molecules are also involved in the formation and stabilization of the supramolecular aggregates of NOMs–NPs associations. Water molecules contribute to the intermolecular attraction between NOMs and NPs fragments, where H–bonds and water bridges formed in both the outer and inner domains of the clusters help to stabilize the hydrophilic functional groups, in good agreement with earlier works [44,72–74].

3.2. Interaction energies between NOMs and NPs

The interaction energies between NOMs and pristine/aged NPs as a function of simulation time are provided (Fig. S6) to clearly delineate the fundamental mechanism leading to the spontaneous clustering and assembly of the two substances. For the NOMs–pristine PE binary system (Fig. S6A), Coulombic energy is close to zero, implying that electrostatic interaction is not favorable for the binding of NOMs to PE particle, and in this case, only vdW interaction is responsible for the hetero–aggregation behavior. For NOMs–virgin PVC and PS assemblages, both vdW and electrostatic forces have contributions, with vdW interactions significantly stronger than electrostatic interactions, suggesting that vdW interactions are the dominant driving force responsible for aggregation between them and electrostatic interactions play a very limited role; furthermore, electrostatic interaction is slightly more important in the NOMs–PVC than in NOMs–PS system (Fig. S6C and E). In conclusion, vdW interactions are mainly responsible for the binding and aggregation between NOMs and unaged NPs, whereas the electrostatic driving force is only important for PVC. This finding is in good agreement with recent studies [75]. These differences can be attributed to the chemical nature of the NP monomers, and our subsequent DFT calculation results will give a direct interpretation of the observed difference.

Positive Coulombic interaction energies indicate unfavorable interactions between NOMs and aged NPs (Fig. S6B, D, and F). This is because both substances are negatively charged due to the deprotonation of carboxyl groups, resulting in an overall repulsive force between them. For these systems, vdW interaction energies are slightly negative (Fig. S6B, D, and F), implying that intermolecular forces mildly contribute to the aggregation between NOMs and aged NPs. These results show that the direct interaction between NOMs and aged NPs is not the dominant factor for their aggregation behavior. Instead, the Ca^{2+} bridging effect attracting and binding to the multiple deprotonated carboxylic groups plays a major role in promoting aggregation (discussed below).

3.3. Local coordination by cation bridging

The bridging effect of cations such as Ca^{2+} has been recognized as a fundamental mechanism for the stabilization and aggregation of NOM fragments that are abundant in deprotonated carboxyl groups in near-neutral pH environments [5,29,76,77]. In comparison, the bridging effect between carboxyl groups of NOMs by Na^{+} is relatively weak, which means the aggregation of NOMs is not effectively promoted by Na^{+}. Consequently, Ca^{2+} cations in a water environment mainly contribute to the aggregation behavior of NOMs and aged NPs. To quantitatively characterize the local coordination structures of Ca^{2+} complexation with deprotonated carboxyl groups (COO^{-}) and to distinguish Ca–bridged homogeneous and heterogeneous aggregation, radial distribution functions (RDFs) were analyzed and presented.

Fig. S7 shows the RDFs curves of aqueous Ca^{2+} with respect to carboxyl O atoms of NOMs and aged NPs, respectively, in binary systems. One can find that the scenarios of Ca^{2+} coordination with carboxyl O of NOMs are very similar in all of the three systems (Fig. S7A, C, and E). In brief, the RDF curves show a sharp and symmetrical peak centered at ~2.60 Å, which corresponds to the average Ca–O ^{carboxyl} bond length, and the accumulating coordination number (CN) of the peak is around 2.1, which indicates that, on average, each Ca^{2+} in solution binds firmly with 2.1 O atoms from NOMs' carboxyl groups. Moreover, in the three binary systems, Ca^{2+} is respectively bound to 0.92, 0.50, and 0.38 carboxyl O of aged PE, PS, and PVC with an average distance of 2.60 Å (Fig. S7B, D, and F). These data show that when NOMs and aged NPs coexist, homogeneous aggregation of both substances still occurs by Ca^{2+} bridging.

Fig. 4 shows the RDF and CN profiles of the C ^{carboxyl} of NOMs surrounded by the C ^{carboxyl} of aged NPs, which helps to better reveal the heterogeneous aggregation between them formed by Ca^{2+} bridging, and also illustrates representative configurations corresponding to the peak positions of the RDF to visually show local polymerizing structures of NOMs–NPs heterogeneous aggregation. A distinct peak or multiple peaks between 3 and 6 Å can be identified in the carboxyl-carboxyl RDF curves (Fig. 4A–C), and the accumulated CN values (at 6.0 Å) reveal that, on average, each carboxyl group in NOMs is associated with 0.27, 0.16, and 0.10 carboxyl groups in aged PE, PS, and PVC, forming multiple carboxyl chelates bridged by Ca^{2+} (Fig. 4D–F) and finally evolving into a heterogeneous aggregate.

To summarize, Ca^{2+} plays a crucial role in the aggregation (homogeneous and heterogeneous) and stabilization of NOMs and aged NPs because the negatively charged carboxyl groups are partially neutralized by Ca^{2+} cations in solution, which reduces the intermolecular and intramolecular charge repulsion and limits conformational expansion, thereby initializing the formation of compact aggregates.

3.4. Quantitative analysis of molecular surface by DFT calculations

3.4.1. Electrostatic potential

The isosurface-colored maps of electrostatic potential (ESP) (Fig. 5) are used to characterize the overall ESP distributions of the six monomeric species of NPs. For virgin PE, it can be found that due to its nonpolar geometry, its vdW surface distributes ESP of nearly zero evenly (Fig. 5A), resulting in the smallest magnitude of ESP among all the NPs. Virgin PVC exhibits a significantly higher ESP scene, with the regions around the Cl atom showing minimum negative ESP and the domains surrounding the H atom presenting maximum positive values (Fig. 5B). Overall, virgin PS has a slightly higher electronegativity than PE and the lowest ESPs, characterized by an annular negative isosurface, are found in the regions between the benzene rings, while other regions exhibit a significantly small magnitude of ESP (Fig. 5C).

Compared to the pristine NPs, the surface ESPs of the aged NPs are distributed in a significantly lower region due to the introduction of non-

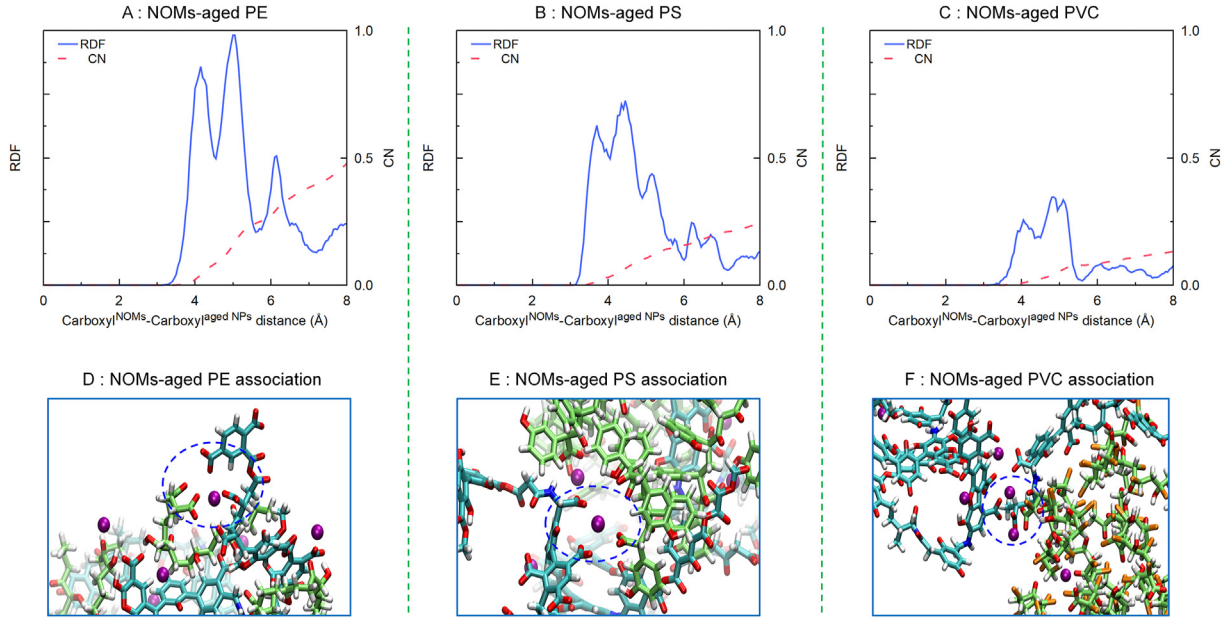

Fig. 4. Radial distribution function (RDF) and coordination number (CN) curves of the carboxyl C of NOMs with respect to the carboxyl C of aged NPs (A–C) and representative hetero–polymerization structures bridged by Ca^{2+} (D–F). N = blue; H = white; O = red; Ca = purple; Cl = orange. C atoms in NOMs and NPs are shown in cyan and green, respectively.

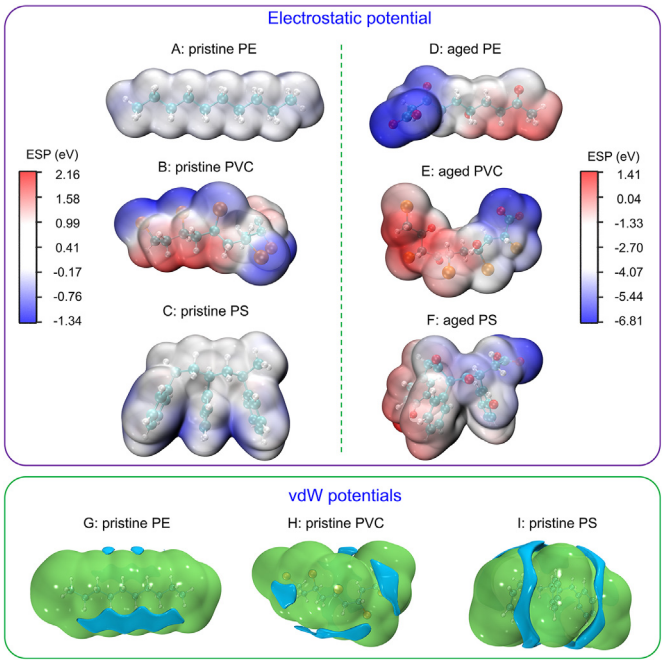

Fig. 5. Isosurface maps of the electrostatic potential (ESP) for (A) pristine PE, (B) pristine PVC, (C) pristine PS, (D) aged PE, (E) aged PVC, and (F) aged PS (isosurface = 0.001 a.u.). Red and blue colors correspond to the positive and negative parts of ESP, respectively. Isosurface maps of vdW potential for (G) pristine PE, (H) pristine PVC, and (I) pristine PS (isovalue = ± 0.75 kcal/mol). Green and blue colors correspond to positive and negative values, respectively.

uniformly distributed oxygen-containing moieties, which are found to increase the non-uniform distribution of the surface ESPs. This, together with the increased H–bonding interactions, promotes the increase in adsorption and aggregation with NOMs. It can be clearly seen that the most negative ESP values are caused by the deprotonated carboxylic groups in all three aged NPs (Fig. 5D–F), indicating that these sites are prone to forming pronounced electrostatic interactions with cations.

3.4.2. *vdW potential*

Due to the low polarity of pristine NPs, their vdW interaction should be of greater importance in comparison to their electrostatic interaction according to chemical intuition. Consequently, the isosurface maps of the vdW potentials of the three pristine NPs are depicted (Fig. 5G–I). This study primarily focused on the blue regions, where the effect of dispersive attraction outweighs that of exchange–repulsion, and generally, the interacting atoms bind to such region. For unaged PE, the negative part of its vdW potential isosurface (blue region) is symmetrically distributed on both sides around C atoms (Fig. 5G). Due to the negative ESP and the polarity generated by the Cl atoms in virgin PVC, the blue region of its vdW potential isosurface is mainly concentrated around C (Fig. 5H). For pristine PS, the blue region is predominantly near the ring center (Fig. 5I). The strong dispersive attraction in this region suggests that π–π stacking interaction plays a pivotal role in its aggregation with NOMs. In fact, strong π–π interactions between PS and NOMs are clearly identified in the MD trajectories. An earlier study also suggested the π–π conjugation for PS interaction with NOMs [23].

3.4.3. *Molecular polarity index (MPI)*

MPI is used to quantify the polarity of molecules with non-uniformly distributed ESP. MPI is calculated by averaging the absolute values of ESPs on the surface of a molecule. A higher MPI indicates a stronger polarity and a greater binding affinity through electrostatic interactions. The calculated MPI values of the six NP monomers are provided in Table S3, and for comparison, the MPI of water molecules is also computed at the same theoretical level. The MPIs for unaged PE, PS, and PVC are 3.1, 8.5, and 22.2 kcal/mol, respectively. Therefore, PE exhibits the lowest polarity, and PS also presents a very low polarity. As a result, it is mainly the vdW interactions, rather than electrostatic interactions, that drive the aggregation of virgin PE and PS. In contrast, the aged NPs are much more polar than their pristine forms, as the derived MPIs are 43.2 kcal/mol for aged PE, 51.6 kcal/mol for aged PS, and 42.2 kcal/mol for PVC. The MPI of the H_2O molecule is found to be 22.1 kcal/mol, which is similar to that of pristine PVC (22.2 kcal/mol) and much higher than that of pristine PE (3.1 kcal/mol) and PS (8.5 kcal/mol). The MPI of H_2O is significantly lower than that of aged NPs (at least 42.2 kcal/mol), and therefore the polarity of the water molecule is much smaller than that of aged NPs, confirming that the strength of electrostatic interactions between aged NPs and NOMs is rather weak.

3.5. *Visualization analysis of weak interactions*

Based on DFT calculations and wavefunction analysis, IGMH is a highly versatile and effective analysis method for identifying and visualizing areas of significant interaction in a wide range of chemical systems. An outstanding advantage of IGMH is the ability to define fragments, so as to exclusively analyze the intermolecular interactions between fragments. Taking the NOM-aged PS system as an example, the DFT geometry optimization method was used to obtain the structure of NOM-aged PS dimer with the initial configuration (1 aged PS molecule + 1 NOM fragment) from the trajectory of MD simulations. According to the acquired structure, IGMH analysis of the two fragments in such a dimer was carried out.

It can be seen that the isosurfaces between aged PS and NOM are largely green (Fig. 6), which implies that slightly low electron density is in the region related to intermolecular interaction, and the molecular binding between the two fragments is predominantly induced by dispersion attraction, since electrostatic interaction normally is accompanied by relatively higher electron density. Although the dispersion interaction between atom pairs is typically assumed to be weak, the isosurfaces between the fragments are notably wide, almost covering the whole interaction region (Fig. 6). This observation could suggest that the vdW interaction between NOM and aged PS fragments is not weak and play a significant role in the binding. Moreover, the isosurfaces located between the rings of NOM and aged PS are stacked parallelly (Fig. 6),

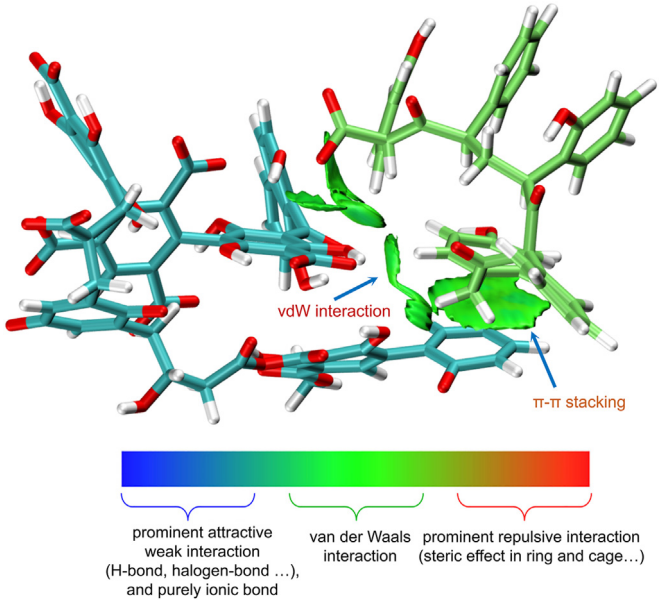

Fig. 6. Sign(λ_2)ρ colored IGMH isosurface map of NOM-aged PS dimer. The NOM monomer and PS monomer are defined as the two fragments in IGMH analysis. $\delta g^{inter} = 0.003$ a.u.

which signifies a significant π–π interaction. The π–π stacking effect is expected to increase the binding strength. However, due to the big structural difference, there is no comparable binding mode or interaction mechanism for PE and PVC. Hence, it can be deduced that for other kinds of NPs that possess a benzene ring, π–π interaction is likely to noticeably intensify their adhesion and aggregation with NOMs.

4. Conclusion

This study investigated the dynamic aggregation and binding mechanisms between NOMs and NPs at the molecular scale. Molecular modeling results showed that the virgin NPs tend to form a homogeneous assembly, which is mainly driven by hydrophobic force and vdW interaction. In contrast, due to the presence of negatively charged carboxyl groups, the homogeneous aggregation of aged NPs is mainly caused by the cation bridging effect, which partially neutralizes the negatively charged carboxylic groups. Pristine PE and PS can easily assemble into a homogenous aggregate, and then NOM molecules tend to be adsorbed on the outer surfaces of such NP particles, then the subsequent NOMs can either bind to the NP surface sites or adhere to the NOM fragments that have already been attached to the NPs. In comparison, NOM fragments are not obviously adsorbed on the homogenous aggregate of virgin PVC due to its relatively higher polarity and the presence of chlorine; instead, NOM molecules tend to self-aggregate and then come into contact with the pristine PVC particle to form an interface. In the case of aged NPs, their interactions with NOMs are governed by a variety of mechanisms, such as intermolecular hydrogen bonding involving hydrophilic functional groups, hydrophobic interactions including π–π stacking, and the cation bridging effect.

CRediT authorship contribution statement

Chi Zhang: Writing – review & editing, Writing – original draft, Funding acquisition, Formal analysis, Data curation, Conceptualization. **Zhiyu Zhou:** Writing – original draft, Methodology, Investigation, Conceptualization. **Mengning Xi:** Software. **Haozhe Ma:** Resources, Methodology. **Junhao Qin:** Writing – review & editing, Supervision. **Hanzhong Jia:** Writing – review & editing, Supervision.

Declaration of competing interests

The authors declare that they have no known competing financial interests or personal relationships that could have appeared to influence the work reported in this paper.

Acknowledgements

This work was supported by the National Natural Science Foundation of China (Grants No. 42107263). We thank the High-Performance Computing Center (HPC) of Northwest A&F University (NWAFU) for providing computing resources and National Center for Supercomputing in Xi'an.

Appendix A. Supplementary data

Supplementary data to this article can be found online at https://doi.org/10.1016/j.eehl.2024.08.004.

References

[1] A.M. Kellerman, D.N. Kothawala, T. Dittmar, L.J. Tranvik, Persistence of dissolved organic matter in lakes related to its molecular characteristics, Nat. Geosci. 8 (6) (2015) 454–457.
[2] J. Lehmann, M. Kleber, The contentious nature of soil organic matter, Nature 528 (7580) (2015) 60–68.
[3] Z. Zhou, C. Zhang, M. Xi, H. Ma, H. Jia, Multi-scale modeling of natural organic matter–heavy metal cations interactions: aggregation and stabilization mechanisms, Water Res. 238 (2023) 120007.
[4] T. Lan, P. Wu, X. Yin, Y. Zhao, J. Liao, D. Wang, et al., Rigidity and flexibility: unraveling the role of fulvic acid in uranyl sorption on graphene oxide using molecular dynamics simulations, Environ. Sci. Technol. 57 (28) (2023) 10339–10347.
[5] D. Petrov, D. Tunega, M.H. Gerzabek, C. Oostenbrink, Molecular dynamics simulations of the standard leonardite humic acid: microscopic analysis of the structure and dynamics, Environ. Sci. Technol. 51 (10) (2017) 5414–5424.
[6] I. Ali, X. Tan, J. Li, C. Peng, I. Naz, Z. Duan, et al., Interaction of microplastics and nanoplastics with natural organic matter (NOM) and the impact of NOM on the sorption behavior of anthropogenic contaminants – a critical review, J. Clean. Prod. 376 (2022) 134314.
[7] J.R. Jambeck, R. Geyer, C. Wilcox, T.R. Siegler, M. Perryman, A. Andrady, et al., Plastic waste inputs from land into the ocean, Science 347 (6223) (2015) 768–771.
[8] B. Gewert, M.M. Plassmann, M. MacLeod, Pathways for degradation of plastic polymers floating in the marine environment, Environ. Sci. Process Impacts 17 (9) (2015) 1513–1521.
[9] R.V. Moharir, S. Kumar, Challenges associated with plastic waste disposal and allied microbial routes for its effective degradation: a comprehensive review, J. Clean. Prod. 208 (2019) 65–76.
[10] D. Hu, M. Shen, Y. Zhang, G. Zeng, Micro(nano)plastics: an un-ignorable carbon source? Sci. Total Environ. 657 (2019) 108–110.
[11] G. Liu, Z. Zhu, Y. Yang, Y. Sun, F. Yu, J. Ma, Sorption behavior and mechanism of hydrophilic organic chemicals to virgin and aged microplastics in freshwater and seawater, Environ. Pollut. 246 (2019) 26–33.
[12] Q. Wang, Y. Zhang, X. Wangjin, Y. Wang, G. Meng, Y. Chen, The adsorption behavior of metals in aqueous solution by microplastics effected by UV radiation, J. Environ. Sci. (China) 87 (2020) 272–280.
[13] M. Shen, Y. Zhu, Y. Zhang, G. Zeng, X. Wen, H. Yi, et al., Micro(nano)plastics: unignorable vectors for organisms, Mar. Pollut. Bull. 139 (2019) 328–331.
[14] A. Pradel, C. Catrouillet, J. Gigault, The environmental fate of nanoplastics: what we know and what we need to know about aggregation, NanoImpact 29 (2023) 100453.
[15] O.S. Alimi, J. Farner Budarz, L.M. Hernandez, N. Tufenkji, Microplastics and nanoplastics in aquatic environments: aggregation, deposition, and enhanced contaminant transport, Environ. Sci. Technol. 52 (4) (2018) 1704–1724.
[16] J. Gigault, H. El Hadri, B. Nguyen, B. Grassl, L. Rowenczyk, N. Tufenkji, et al., Nanoplastics are neither microplastics nor engineered nanoparticles, Nat. Nanotechnol. 16 (5) (2021) 501–507.
[17] S. Lambert, M. Wagner, Characterisation of nanoplastics during the degradation of polystyrene, Chemosphere 145 (2016) 265–268.
[18] Y. Liu, Y. Wang, X. Ling, Z. Yan, D. Wu, J. Liu, et al., Effects of nanoplastics and butyl methoxydibenzoylmethane on early zebrafish embryos identified by single-cell RNA sequencing, Environ. Sci. Technol. 55 (3) (2021) 1885–1896.
[19] Z. Wang, X. Xing, M. Xue, S. Bai, P. Li, C. Li, et al., Insights into heteroaggregation of polystyrene nanoplastics with hematite nanoparticles and configuration-dependent adsorption for PFOA and PFOS, Colloids Surf., A 649 (2022) 129467.
[20] Y. Zhang, Y. Luo, X. Yu, D. Huang, X. Guo, L. Zhu, Aging significantly increases the interaction between polystyrene nanoplastic and minerals, Water Res. 219 (2022) 118544.
[21] Y. Mao, H. Li, X. Huangfu, Y. Liu, Q. He, Nanoplastics display strong stability in aqueous environments: insights from aggregation behaviour and theoretical calculations, Environ. Pollut. 258 (2020) 113760.
[22] N. Singh, E. Tiwari, N. Khandelwal, G.K. Darbha, Understanding the stability of nanoplastics in aqueous environments: effect of ionic strength, temperature, dissolved organic matter, clay, and heavy metals, Environ. Sci.: Nano 6 (10) (2019) 2968–2976.
[23] L. Ding, Y. Luo, X. Yu, Z. Ouyang, P. Liu, X. Guo, Insight into interactions of polystyrene microplastics with different types and compositions of dissolved organic matter, Sci. Total Environ. 824 (2022) 153883.
[24] Y. Yin, M. Shen, Z. Tan, S. Yu, J. Liu, G. Jiang, Particle coating-dependent interaction of molecular weight fractionated natural organic matter: impacts on the aggregation of silver nanoparticles, Environ. Sci. Technol. 49 (11) (2015) 6581–6589.
[25] O. Oriekhova, S. Stoll, Heteroaggregation of nanoplastic particles in the presence of inorganic colloids and natural organic matter, Environ. Sci.: Nano 5 (3) (2018) 792–799.
[26] J. Greathouse, K. Johnson, H. Greenwell, Interaction of natural organic matter with layered minerals: recent developments in computational methods at the nanoscale, Minerals 4 (2) (2014) 519–540.
[27] D. Devarajan, L. Liang, B. Gu, S.C. Brooks, J.M. Parks, J.C. Smith, Molecular dynamics simulation of the structures, dynamics, and aggregation of dissolved organic matter, Environ. Sci. Technol. 54 (21) (2020) 13527–13537.
[28] A.G. Kalinichev, E. Iskrenova-Tchoukova, W.Y. Ahn, M.M. Clark, R.J. Kirkpatrick, Effects of Ca^{2+} on supramolecular aggregation of natural organic matter in aqueous solutions: a comparison of molecular modeling approaches, Geoderma 169 (2011) 27–32.
[29] Y. Zhang, X. Liu, C. Zhang, X. Lu, A combined first principles and classical molecular dynamics study of clay-soil organic matters (SOMs) interactions, Geochem. Cosmochim. Acta 291 (2020) 110–125.
[30] J. Liang, P. Zhen, P. Gan, Y. Li, M. Tong, W. Liu, DFT calculation of nonperiodic small molecular systems to predict the reaction mechanism of advanced oxidation processes: challenges and perspectives, ACS ES&T Eng 4 (1) (2024) 4–18.

[31] F. Li, A.G.L. Borthwick, W. Liu, Environmental theoretical calculation for non-periodic systems, Trends Chem. 5 (6) (2023) 410–414.
[32] M. He, X. Liu, X. Lu, Y. Zhang, R. Wang, Structure, stability, and acidity of the uranyl arsenate dimer in aqueous solution, Inorg. Chem. 62 (22) (2023) 8729–8738.
[33] M. He, X. Liu, J. Cheng, X. Lu, C. Zhang, R. Wang, Uranyl arsenate complexes in aqueous solution: insights from first-principles molecular dynamics simulations, Inorg. Chem. 57 (10) (2018) 5801–5809.
[34] Q. Xue, Z. Jiao, W. Pan, X. Liu, J. Fu, A. Zhang, Multiscale computational simulation of pollutant behavior at water interfaces, Water Res. 250 (2024) 121043.
[35] Y. Chen, H. Li, Y. Yin, S. Shan, T. Huang, H. Tang, Effect of microplastics on the adherence of coexisting background organic contaminants to natural organic matter in water, Sci. Total Environ. 905 (2023) 167175.
[36] K. Zhu, H. Jia, S. Zhao, T. Xia, X. Guo, T. Wang, et al., Formation of environmentally persistent free radicals on microplastics under light irradiation, Environ. Sci. Technol. 53 (14) (2019) 8177–8186.
[37] Y. Luo, Y. Zhang, Y. Xu, X. Guo, L. Zhu, Distribution characteristics and mechanism of microplastics mediated by soil physicochemical properties, Sci. Total Environ. 726 (2020) 138389.
[38] K. Zhu, Y. Sun, W. Jiang, C. Zhang, Y. Dai, Z. Liu, et al., Inorganic anions influenced the photoaging kinetics and mechanism of polystyrene microplastic under the simulated sunlight: role of reactive radical species, Water Res. 216 (2022) 118294.
[39] Y. Escalona, D. Petrov, C. Oostenbrink, Vienna soil organic matter modeler 2 (VSOMM2), J. Mol. Graphics Modell. 103 (2021) 107817.
[40] A. Sündermann, R. Solc, D. Tunega, G. Haberhauer, M.H. Gerzabek, C. Oostenbrink, Vienna Soil-Organic-Matter Modeler—generating condensed-phase models of humic substances, J. Mol. Graphics Modell. 62 (2015) 253–261.
[41] Y. Chen, H. Tang, Y. Cheng, T. Huang, B. Xing, Interaction between microplastics and humic acid and its effect on their properties as revealed by molecular dynamics simulations, J. Hazard Mater. 455 (2023) 131636.
[42] D. Van Der Spoel, E. Lindahl, B. Hess, G. Groenhof, A.E. Mark, H.J. Berendsen, GROMACS: fast, flexible, and free, J. Comput. Chem. 26 (16) (2005) 1701–1718.
[43] Y. Duan, C. Wu, S. Chowdhury, M.C. Lee, G. Xiong, W. Zhang, et al., A point-charge force field for molecular mechanics simulations of proteins based on condensed-phase quantum mechanical calculations, J. Comput. Chem. 24 (16) (2003) 1999–2012.
[44] U. Essmann, L. Perera, M.L. Berkowitz, T. Darden, H. Lee, L.G. Pedersen, A smooth particle mesh Ewald method, J. Chem. Phys. 103 (19) (1995) 8577–8593.
[45] H.J.C. Berendsen, J.R. Grigera, T.P. Straatsma, The missing term in effective pair potentials, J. Phys. Chem. C 91 (24) (1987) 6269–6271.
[46] B. Hess, H. Bekker, H.J.C. Berendsen, J.G.E.M. Fraaije, LINCS: a linear constraint solver for molecular simulations 18 (12) (1997) 1463–1472.
[47] Berendsen, J.P.M. Postma, W.F. van Gunsteren, A. DiNola, J.R. Haak, Molecular dynamics with coupling to an external bath, J. Chem. Phys. 81 (8) (1984) 3684–3690.
[48] G. Bussi, D. Donadio, M. Parrinello, Canonical sampling through velocity rescaling, J. Chem. Phys. 126 (1) (2007) 014101.
[49] F. Weigend, R. Ahlrichs, Balanced basis sets of split valence, triple zeta valence and quadruple zeta valence quality for H to Rn: design and assessment of accuracy, Phys. Chem. Chem. Phys. 7 (18) (2005) 3297–3305.
[50] A.D. Becke, Density-functional thermochemistry. III. The role of exact exchange, J. Chem. Phys. 98 (7) (1993) 5648–5652.
[51] C. Lee, W. Yang, R.G. Parr, Development of the Colle-Salvetti correlation-energy formula into a functional of the electron density, Phys. Rev. B Condens. Matter 37 (2) (1988) 785–789.
[52] S. Grimme, J. Antony, S. Ehrlich, H. Krieg, A consistent and accurate ab initio parametrization of density functional dispersion correction (DFT-D) for the 94 elements H-Pu, J. Chem. Phys. 132 (15) (2010) 154104.
[53] T. Lu, F. Chen, Multiwfn: a multifunctional wavefunction analyzer, J. Comput. Chem. 33 (5) (2012) 580–592.
[54] M. Schauperl, P.S. Nerenberg, H. Jang, L.-P. Wang, C.I. Bayly, D.L. Mobley, et al., Non-bonded force field model with advanced restrained electrostatic potential charges (RESP2), Commun. Chem. 3 (1) (2020) 44.
[55] R.F.W. Bader, M.T. Carroll, J.R. Cheeseman, C. Chang, Properties of atoms in molecules: atomic volumes, J. Am. Chem. Soc. 109 (26) (1987) 7968–7979.
[56] T. Lu, Q. Chen, van der Waals potential: an important complement to molecular electrostatic potential in studying intermolecular interactions, J. Mol. Model. 26 (11) (2020) 315.
[57] T. Lu, Q. Chen, Independent gradient model based on Hirshfeld partition: a new method for visual study of interactions in, chemical systems 43 (8) (2022) 539–555.
[58] W. Humphrey, A. Dalke, K. Schulten, VMD: visual molecular dynamics, J. Mol. Graph. 14 (1) (1996) 33–38.
[59] T.D. Kuehne, M. Iannuzzi, M. Del Ben, V.V. Rybkin, P. Seewald, F. Stein, et al., CP2K: an electronic structure and molecular dynamics software package - quickstep: Efficient and accurate electronic structure calculations, J. Chem. Phys. 152 (19) (2020) 194103.
[60] B.G. Lippert, J. Hutter, M. Parrinello, A hybrid Gaussian and plane wave density functional scheme, Mol. Phys. 92 (92) (1997) 477–487.
[61] J.P. Perdew, K. Burke, M. Ernzerhof, Generalized gradient approximation made simple, Phys. Rev. Lett. 77 (18) (1996) 3865–3868.
[62] J. VandeVondele, J. Hutter, Gaussian basis sets for accurate calculations on molecular systems in gas and condensed phases, J. Chem. Phys. 127 (11) (2007) 114105.
[63] S. Goedecker, M. Teter, J. Hutter, Separable dual-space Gaussian pseudopotentials, Phys. Rev. B Condens. Matter 54 (3) (1996) 1703–1710.
[64] R.H. Byrd, P. Lu, J. Nocedal, C. Zhu, A limited memory algorithm for bound constrained optimization 16 (5) (1995) 1190–1208.
[65] O. Andreussi, I. Dabo, N. Marzari, Revised self-consistent continuum solvation in electronic-structure calculations, J. Chem. Phys. 136 (6) (2012) 064102.
[66] Q. Sun, The hydrophobic effects: our current understanding, Molecules 27 (20) (2022) 7009.
[67] A.J.A. Aquino, D. Tunega, G.E. Schaumann, G. Haberhauer, M.H. Gerzabek, H. Lischka, The functionality of cation bridges for binding polar groups in soil aggregates, Int. J. Quant. Chem. 111 (7–8) (2010) 1531–1542.
[68] E. Galicia-Andrés, C. Oostenbrink, M.H. Gerzabek, D. Tunega, On the adsorption mechanism of humic substances on kaolinite and their microscopic structure, Minerals 11 (10) (2021) 1138.
[69] Y. Escalona, D. Petrov, E. Galicia-Andrés, C. Oostenbrink, Exploring the macroscopic properties of humic substances using modeling and molecular simulations, Agronomy 13 (4) (2023) 1044.
[70] X. Wang, X. Wang, W. Zhu, L. Ding, X. Liang, R. Wu, et al., Insight into interactions between microplastics and fulvic acid: mechanisms affected by microplastics type, Sci. Total Environ. 913 (2024) 169427.
[71] A. Abdurahman, K. Cui, J. Wu, S. Li, R. Gao, J. Dai, et al., Adsorption of dissolved organic matter (DOM) on polystyrene microplastics in aquatic environments: kinetic, isotherm and site energy distribution analysis, Ecotoxicol. Environ. Saf. 198 (2020) 110658.
[72] A.J.A. Aquino, D. Tunega, H. Pašalić, G.E. Schaumann, G. Haberhauer, M.H. Gerzabek, et al., Molecular dynamics simulations of water molecule-bridges in polar domains of humic acids, Environ. Sci. Technol. 45 (19) (2011) 8411–8419.
[73] J. Kučerík, P. Ondruch, Y. Kunhi Mouvenchery, G.E. Schaumann, Formation of water molecule bridges governs water sorption mechanisms in soil organic matter, Langmuir 34 (40) (2018) 12174–12182.
[74] M. Boyle, Jr., W.T. Frankenberger, L.H. Stolzy, The influence of organic matter on soil aggregation and water infiltration 2 (4) (1989) 290–299.
[75] W. Liu, H. Tang, B. Yang, C. Li, Y. Chen, T. Huang, Molecular level insight into the different interaction intensity between microplastics and aromatic hydrocarbon in pure water and seawater, Sci. Total Environ. 862 (2023) 160786.
[76] E. Iskrenova-Tchoukova, A.G. Kalinichev, R.J. Kirkpatrick, Metal cation complexation with natural organic matter in aqueous solutions: molecular dynamics simulations and potentials of mean force, Langmuir 26 (20) (2010) 15909–15919.
[77] A.G. Kalinichev, R.J. Kirkpatrick, Molecular dynamics simulation of cationic complexation with natural organic matter 58 (4) (2007) 909–917.